Soft Matter

RSC Publishing

PAPER

View Article Online
View Journal

Semi-flexible polymer chains in quasi-one-dimensional confinement: a Monte Carlo study on the square lattice

Cite this: DOI: 10.1039/c3sm51202a

Hsiao-Ping Hsu* and Kurt Binder

Single semi-flexible polymer chains are modeled as self-avoiding walks (SAWs) on the square lattice with every 90° kink requiring an energy ε_b. While for $\varepsilon_b = 0$ this is the ordinary SAW, varying the parameter $q_b = \exp(-\varepsilon_b/k_BT)$ allows the variation of the effective persistence length ℓ_p over about two decades. Using the pruned-enriched Rosenbluth method (PERM), chain lengths up to about $N = 10^5$ steps can be studied. In previous work it has already been shown that for contour lengths $L = N\ell_b$ (the bond length ℓ_b is the lattice spacing) of order ℓ_p a smooth crossover from rods to two-dimensional self-avoiding walks occurs, with radii $R \propto \ell_p^{1/4}L^{3/4}$, the Gaussian regime predicted by the Kratky–Porod model for worm-like chains being completely absent. In the present study, confinement of such chains in strips of width D is considered, varying D from 4 to 320 lattice spacings. It is shown that for narrow strips ($D < \ell_p$) the effective persistence length of the chains (in the direction parallel to the confining boundaries) scales like ℓ_p^2/D, and $R_\parallel \propto L$ (with a pre-factor of order unity). For very wide strips, $D \gg \ell_p$, the two-dimensional SAW behavior prevails for chain lengths up to $L_{cross} \propto \ell_p(D/\ell_p)^{4/3}$, while for $L \gg L_{cross}$ the chain is a string of blobs of diameter D, *i.e.* $R_\parallel \propto L(\ell_p/D)^{1/3}$. In the regime $D < \ell_p$, the chain is a sequence of straight sequences with length of the order ℓ_p^2/D parallel to the boundary, separated by sequences with length < D perpendicular to the boundary; thus Odijk's deflection length plays no role for discrete bond angles.

Received 30th April 2013
Accepted 26th June 2013

DOI: 10.1039/c3sm51202a

www.rsc.org/softmatter

1 Introduction

Semi-flexible macromolecules (such as double-stranded DNA and other biomolecules) confined in nanoscopic channels have gained enormous interest recently, in experiments,[1–8] analytical theory,[9–28] and computer simulations.[29–32] If the diameter D of the (cylindrical) channel is much larger than the persistence length ℓ_p of the semi-flexible polymer, one expects a situation similar to the case of flexible chains confined in tubes; the chain forms a one-dimensional string of blobs along the channel. For a flexible chain, where ℓ_p is of the order of the bond length, one needs to account for excluded volume interactions in the case of good solvent conditions.[33] Then the number of monomers per blob g is estimated as $g = (D/\ell_b)^{1/\nu}$ where $\nu \approx 0.588$ (in $d = 3$ dimensions)[34] is the critical exponent characterizing the size of an isolated swollen polymer coil,[33] and pre-factors of order unity are ignored throughout. For a chain with N effective monomeric units, then according to this scaling argument,[35] the number of blobs in the string is

$$n = N/g = N(\ell_b/D)^{1/\nu} \quad (1)$$

and the chain extension along the tube is

$$R_\parallel = nD = N\ell_b(\ell_b/D)^{1/\nu-1} \approx N\ell_b(\ell_b/D)^{2/3} \quad (2)$$

where in the last step the Flory approximation[33] $\nu = 3/5$ was used. If one considers the analogous problem in $d = 2$ space dimensions, for a chain confined in a slit of width D in a plane, the argument is identical, the only difference being that $\nu = 3/4$ and hence

$$n = N(\ell_b/D)^{4/3},\ R_\parallel = N\ell_b(\ell_b/D)^{1/3},\ d = 2. \quad (3)$$

One can also consider the (entropic) force per monomer exerted on the confining wall, and then finds

$$f = k_BTD^{-1-1/\nu}. \quad (4)$$

If one considers flexible polymers confined within parallel repulsive walls in $d = 3$ space dimensions, eqn (1) still remains valid, but now the chain conformation rather is characterized by a two-dimensional self-avoiding walk (SAW) of n blobs of diameter D, *i.e.*

$$R_\parallel = Dn^{3/4} = \ell_bN^{3/4}(\ell_b/D)^{-1+3/(4\nu)} \approx \ell_bN^{3/4}(\ell_b/D)^{1/4}. \quad (5)$$

The result for the force on the walls {eqn (4)} remains the same, the free energy (in units of k_BT) simply is given by n, since each blob contributes k_BT.

This picture gets clearly modified when we consider semi-flexible chains, where the persistence length ℓ_p enters as an additional length scale.[36–38] As is well-known, this concept of a persistence length is valid for perfectly Gaussian chains with no

Institut für Physik, Johannes Gutenberg-Universität Mainz, Staudinger Weg 7, D-55099 Mainz, Germany. E-mail: hsu@uni-mainz.de

interactions among the beads whatsoever, while for more realistic models of polymers different definitions for the persistence length disagree,[39] some simply being unsuitable. Since we wish to define the persistence length such that it reflects only the "intrinsic" chain stiffness and does not depend on the contour length $L = (N-1)\ell_b$ of the chain, we shall define ℓ_p here from the average $\langle \cos\theta \rangle$ where θ is the angle between subsequent bonds of the chain,

$$\ell_p = -\ell_b / \ln\langle \cos\theta \rangle. \quad (6)$$

Note that this choice is equivalent to the use of the initial slope of the decay of the bond angle correlation function $\langle \cos\theta(s) \rangle$, for bonds that are s steps apart from the chain contour, $\langle \cos\theta(s) \rangle = \exp(-s\ell_b/\ell_p)$, for small $s\ell_b/\ell_p$; the asymptotic decay of $\langle \cos\theta(s) \rangle$ for large s cannot be used, since it is described by a power law,[40] $\langle \cos\theta(s) \rangle \propto s^{-\beta}$ (with $\beta = 1/2$ in $d = 2$ dimensions[40,41]). We also recall that in the description of the standard continuum model of semi-flexible polymers, the Kratky–Porod model,[42] the persistence length is related to the bending stiffness κ (in units of temperature) as

$$\ell_p = 2\kappa/(d-1). \quad (7)$$

The Kratky–Porod model describes the energy function $\mathscr{H}$ of a chain molecule described by a curve $\vec{r}(s)$ for its contour in continuum space as

$$\mathscr{H}_{KP}\left\{\vec{r}(s)\right\} = \frac{\kappa}{2}\int_0^L \mathrm{d}s \left(\frac{\partial^2 \vec{r}}{\partial s^2}\right)^2. \quad (8)$$

The Kratky–Porod model describes the crossover from rod-like behavior (for $L \leq \ell_p$) to Gaussian random coil-like behavior (for $L \gg \ell_p$). Although in general this model is commonly used for the description of semi-flexible polymers (see *e.g.* ref. 43 and refs. therein), it has been shown[41] to be rather unsuitable in $d = 2$. Specifically, the mean square end-to-end distance $\langle R^2 \rangle$ of the polymer has been shown to cross over at $L \approx \ell_p$ from the (trivial!) rod-like behavior $\langle R^2 \rangle = L^2$ (for $L < \ell_p$) to the $d = 2$ SAW behavior (omitting again an unimportant non-universal constant of order unity)

$$\langle R^2 \rangle = \ell_p{}^{1/2} L^{3/2},\ L \gg \ell_p. \quad (9)$$

The predicted Gaussian behavior ($\langle R^2 \rangle = 2\ell_p L$) is completely absent[41] in $d = 2$.

When we now consider the confinement of a semi-flexible chain in $d = 2$ in a slit of width D, eqn (3) is easily generalized for $D \gg \ell_p$. The chain still forms a string of blobs of diameter D, the number n of these blobs and the extension $R_\parallel$ of the chain along the slit being

$$n = L/L_{cross},\ L_{cross}/\ell_p = (D/\ell_p)^{4/3},\ R_\parallel = L(\ell_p/D)^{1/3}. \quad (10)$$

Thus we see that scaling predicts essentially the role of the bond length ℓ_b taken over by the persistence length. However, more interesting is the behavior when $\ell_b \ll D < \ell_p$; the slit is too narrow to allow the formation of blobs with $d = 2$ SAW statistics. The excluded volume effects are not important, when we assume that the chain is essentially stretched out along the slit (hairpin formation[25] shall be disregarded here). However, still the chain is not simply stretched out according to a straight line (which would lead to simple rod behaviors $R_\parallel = L$) but deviates due to bending fluctuations from such a straight line. Using eqn (8) Odijk[12] derived that the length scale over which the chain follows an essentially straight path, but inclined relative to the x-axis along the slit, is

$$\lambda = (D^2\ell_p)^{1/3}\ (\lambda < \ell_p \text{ for } D < \ell_p), \quad (11)$$

and typical angles that the chain makes with the x-axis then are of order $\theta \approx D/\lambda = (D/\ell_p)^{1/3}$. Odijk[12] also derived the free energy cost of confinement as

$$\Delta F/k_B T \approx (L/\lambda)\ln(\ell_p/\lambda)\ (\text{for } L \geq \ell_p \text{ and } \ell_p \gg \lambda). \quad (12)$$

In the present paper, we present extensive Monte Carlo simulations using the pruned-enriched Rosenbluth method (PERM)[44,45] to study this problem of confined two-dimensional semi-flexible polymers for the model of self-avoiding walks on the square lattice, including an energy penalty ε_b whenever the SAW makes a kink. In previous work this model has been studied in the absence of any confinement, and it has been shown that ℓ_p can be conveniently varied from the fully flexible case (where ℓ_p is of the order of the lattice spacing) to the order of 100 lattice spacings.[41,46] Our main focus, of course, is on the nontrivial regime where D and ℓ_p are of the same order, where all theoretical predictions sketched above {eqn (10)–(12)} clearly are doubtful. We also note that for $\varepsilon_b = 0$ this model has been used very successfully to test eqn (3) and (4) describing confinement of flexible chains.[47]

In the following section, we briefly summarize the simulation method. Then we describe our results, and the concluding section gives the summary and outlook.

2 Simulation method

Our model is the SAW on the square lattice, where each effective monomer occupies a lattice site, the bond length between the nearest neighbors along the chain (ℓ_b) is just the lattice spacing, and this is henceforth our unit of length. The excluded volume is accounted for by the fact that double occupancy of lattice sites is forbidden. Using the standard bond bending potential $U_b = \varepsilon_b(1 - \cos\theta)$, where θ is the angle between subsequent bond vectors along the chain, the problem is enormously simplified by the fact that only angles $\theta = 0^\circ$ and $\pm 90^\circ$ are possible on the square lattice. Thus no energy cost arises if the bond vector continues along the direction of the previous one, while every kink costs the same energy ε_b. Thus, the partition sum can be expressed as a polynomial in the Boltzmann factor $q_b = \exp(-\varepsilon_b/k_B T)$,

$$Z_N(q_b, D) = \sum_{\text{config}} C_{N,N_{bend}}(q_b, D) q_b^{N_{bend}}, \quad (13)$$

where the sum over configurations includes all SAWs with y-coordinates of the monomers in the range $1 \leq y \leq D$, to realize

Table 1 Estimates of the persistence length $\ell_p(q_b)$ (eqn (6)), the fugacity per monomer $\mu_\infty(q_b)$ (eqn (13)), and the amplitude $C(q_b)$ of the end-to-end distance ($\sqrt{\langle R^2\rangle} = C(q_b)N^{3/4}$) as $N \to \infty$ for semi-flexible chains in the bulk

q_b	ℓ_p	μ_∞	$C(q_b)$
1.0	1.06	0.37905227(6)	0.8765(4)
0.4	2.00	0.60046275(8)	0.9778(8)
0.2	3.50	0.74878796(8)	1.098(5)
0.1	6.46	0.85568975(5)	1.262(5)
0.05	12.35	0.92201161(5)	1.412(3)
0.03	20.21	0.95163915(8)	1.662(7)
0.02	30.02	0.96720943(5)	1.825(7)
0.01	59.22	0.98331993(7)	2.166(4)
0.005	118.22	0.99158684(9)	2.565(4)

the confinement. That is, following previous work on flexible SAWs the walls[47] are placed at $y = 0$ and $y = D + 1$.

We apply the pruned enriched Rosenbluth method (PERM)[44–47] which is a chain growth algorithm with population control and depth-first implementation. Details about this algorithm can be found in a recent review.[45] This algorithm allows the study of the chain length up to about $N = 10^5$, for a wide variety of chain stiffnesses, varying q_b from $q_b = 1$ (flexible chains) to $q_b = 0.005$. Table 1 gives an overview of the corresponding persistence lengths $\ell_p(q_b)$ in the bulk, as well as the fugacity $\mu_\infty(q_b)$ per monomer (defined as $\ln \mu_\infty(q_b) = -(1/N)\ln[Z_N(q_b)/N^{\gamma-1}]$ with $\gamma = 43/32$) and the amplitude $C(q_b)$ of the end-to-end distance, $\sqrt{\langle R^2\rangle} = C(q_b)N^{3/4}$ as $N \to \infty$. Related data can be found in ref. 46. The confined chains studied in the present work refer to the choices $D = 4$, 8, 10, 16, 20, 32, 40, 64, 80, 160 and 320.

Finally we note that when the excluded volume is neglected (apart from forbidding immediate reversals of the SAW) one finds easily that $\langle \cos\theta\rangle = 1/(1 + 2q_b)$ and hence $\ell_p \approx 1/(2q_b)$ for small q_b. The data of Table 1 rather imply[46] $\ell_p \approx 0.61/q_b$.

3 Simulation results and their use for the test of the scaling predictions

3.1 Flexible chains

While the confinement of flexible SAWs in $d = 2$ has already been considered in ref. 47, we extend these results here since it is necessary to compare the behavior of semi-flexible chains and flexible ones in order to elucidate the effects of chain stiffness. Fig. 1 summarizes our main results; (for very long chains, up to $N = 128\,000$) one can see that the fugacity μ_D per monomer, the rescaled x-component of the end-to-end distance $\langle \Delta x\rangle/N$ and the density ρ_b of wall contacts satisfy simple power laws as a function of D in the thermodynamic limit, *i.e.*, as $N \to \infty$, Fig. 1a,

$$\mu_D - \mu_\infty \approx 0.737 D^{-4/3}, \quad (14)$$

$$\langle \Delta x\rangle/N \approx 0.915 D^{-1/3}, \quad (15)$$

$$\rho_b = [n(y = 1) + n(y = D)]/2\langle \Delta x\rangle \approx 10.75 D^{-2}. \quad (16)$$

Here $n(y = 1)$ and $n(y = D)$ are the average numbers of monomers adjacent to the wall. Note that ρ_b can be simply related to the pressure exerted on the wall, since the force f per monomer can be written as ($k_BT \equiv 1$)

$$f = \frac{1}{N}\frac{\partial \ln Z_N(q_b, D)}{\partial D} \propto D^{-1-1/\nu} = D^{-7/3}, \quad (17)$$

using the fact that $\ln \mu_D(q_b) = -\ln Z_N(q_b,D)/N$ and eqn (14), recalling that $\nu = 3/4$ in $d = 2$. Thus eqn (17) justifies eqn (4). Since the pressure p on the wall is the force per unit length rather than per monomer, we can write $p = Nf/\langle \Delta x\rangle$ to find that $p \propto \rho_b$. Thus eqn (16) verifies eqn (4) and (17), while eqn (15) verifies eqn (3); note that $\ell_b \equiv 1$ in our model. Thus Fig. 1a shows that for flexible SAW's these scaling relationships hold essentially true for D as small as a few lattice spacings, and the amplitude prefactors are of order unity.

It is remarkable to note that the density in the boundary layers ρ_b is much smaller than the average monomer density in the region of the "string of blobs" taken by the chain, which is $\rho_{av} = \langle \Delta x\rangle/(ND) \propto D^{-4/3}$. This result already implies that the density profile across the film is very nonuniform, as actually observed (Fig. 1b). In ref. 47 a phenomenological expression for the scaling function describing $\rho(y)$ was proposed as follows:

$$\rho(y) = \frac{1}{D+1} f_\rho(\xi) \equiv \frac{1}{D+1} A[\xi(1-\xi)]^{4/3}, \quad \xi = y/(D+1). \quad (18)$$

Of course, there is a slight arbitrariness in the precise normalization of transverse distances y; here we have defined the scaling variable ξ by dividing y with the geometrical distance $D + 1$ between the two walls. One could have introduced a kind of "extrapolation length" δ, writing rather $\xi = (y - \delta)/(D + 1 - 2\delta)$, where δ is of order unity.[47] However, this does not improve the quality of the fit significantly.

Fig. 1c demonstrates a similar scaling proposed for the lateral distribution of the chain ends $\rho_e(y)$, described as[47]

$$\rho_e(y) = \frac{1}{D+1} f_e(\xi) \equiv \frac{1}{D+1} A_e [\xi(1-\xi)]^{25/48}. \quad (19)$$

The result that $\rho_e(y) \propto y^{25/48}$ has been rigorously derived from the conformal invariance[48] and has motivated eqn (19), where A_e (just as A in eqn (18)) is an adjustable amplitude factor.

Finally, Fig. 1d shows the mean square end-to-end distance in the direction parallel to the confining boundary, in a scaling plot normalized such that unconfined chains tend to a constant while confined chains exhibit the power law, eqn (3). Note that all data irrespective of the chain length N collapse on a master curve $\tilde{P}_\parallel$ when we rescale variables in terms of the radius R_0 of an unconfined two-dimensional SAW, with $R_0 = N^{3/4}$ (absorbing a prefactor in the normalization)

$$\langle R_\parallel{}^2\rangle/R_0{}^2 = \tilde{P}_\parallel(\zeta),\ \zeta = R_0/(D+1) = \mathrm{N}^{3/4}/(D+1). \quad (20)$$

For large ζ we have $\tilde{P}(\zeta) \propto \zeta^{2/3}$ and hence $\langle R_\parallel{}^2\rangle \propto N^{3/2}N^{1/2}/(D+1)^{2/3} = (N/(D+1)^{1/3})^2$, which for large D is equivalent to eqn (3), as it should be. A similar scaling function applies to the component $\langle R_\perp{}^2\rangle$ in the y-direction as well, $\langle R_\perp{}^2\rangle/\langle R_0{}^2\rangle = \tilde{P}_\perp(\zeta)$ with $\tilde{P}_\perp(\zeta) \propto \zeta^{-2}$ for $\zeta \gg 1$ (not shown here to save

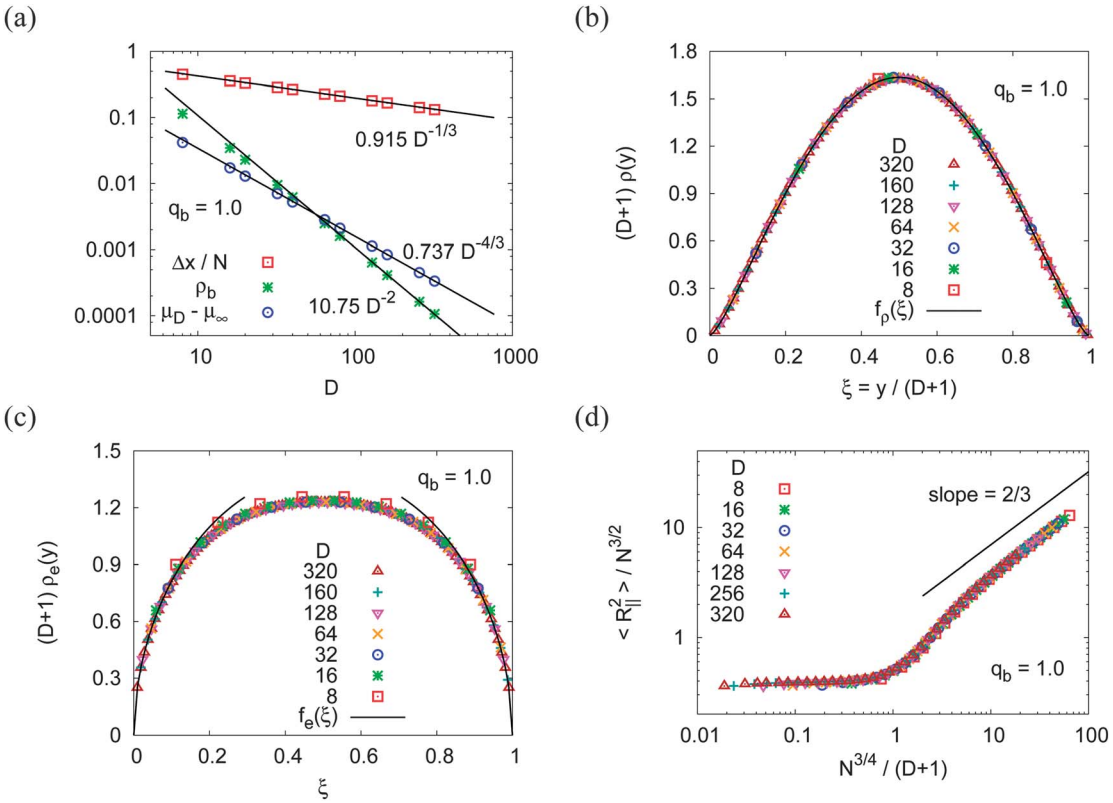

Fig. 1 (a) Log–log plot of $\mu_D - \mu_\infty$, $\langle \Delta x \rangle / N$, and ρ_b *versus* D as $N \to \infty$. The straight lines are the power laws quoted in eqn (14)–(16). All data are for $q_b = 1$. (b) Rescaled monomer density profile $(D + 1)\rho(y)$ *versus* $\xi = y/(D + 1)$. The full curve shows eqn (18) with the amplitude factor $A = 10.38$. (c) Rescaled profile of the density of the chain ends, $(D + 1)\rho_e(y)$ *versus* ξ. The full curve shows eqn (19) with the amplitude factor $A_e = 2.85$. (d) Rescaled mean square end-to-end distance $\langle R_\parallel^2 \rangle / N^{3/2}$ parallel to the boundaries *versus* the scaling variable $N^{3/4}/(D + 1)$. The straight line shows the slope 2/3, which corresponds to eqn (3). All data are for $q_b = 1.0$ and for D ranging from $D = 8$ to $D = 320$, as indicated. In (b)(c)(d), all data are for $q_b = 1$, and for D ranging from $D = 8$ ($N = 5000$) to $D = 320$ ($N = 128\,000$).

space). In any case, we conclude that the behavior of confined flexible chains in $d = 2$ dimensions can be understood in full detail.

3.2 The persistence length of confined semi-flexible chains

In Section II we have seen that the persistence length ℓ_p is related inversely to the Boltzmann factor $q_b = \exp(-\varepsilon_b/k_BT)$ for the walk to make a kink, $\ell_p \approx 0.61/q_b$. However, when ℓ_p exceeds D, the walk must predominantly run along the x-axis; whenever a kink occurs so that the walk starts to run along the y-axis, a second kink must soon occur so that the walk continues along the x-axis again. So the picture of the chain consists of long straight segments (of length $\ell_p(D)$) oriented along the x-axis, separated by short pieces (of a length smaller than D) oriented along the y-axis, involving two kinks, one kink from $\varphi = 0°$ to $\varphi = \pm 90°$ and then a second kink back to $\varphi = 0°$ again. Such-defects containing two neighboring kinks (which would annihilate each other when they meet) clearly involve an activation energy of $2\varepsilon_b$, their probability to occur hence scales as q_b^2 or ℓ_p^{-2}. This consideration suggests to consider a scaling hypothesis for $\ell_p(D)$ in the form (henceforth we denote $\ell_p(D = \infty)$ simply as ℓ_p throughout)

$$\ell_p(D) = \ell_p \tilde{P}_L(\ell_p/D) \tag{21}$$

with a scaling function $\tilde{P}_L(\eta)$ which scales as $\tilde{P}_L(\eta) \approx 1$ for $\eta \ll 1$ but $\tilde{P}_L(\eta) \propto \eta$ for $\eta \gg 1$.

Fig. 2 tests this idea with our simulation data for various values of q_b (and hence ℓ_p, *cf.* Table 1), and furthermore shows that ℓ_p/D is a useful scaling variable to describe the rescaled fugacity per monomer $[\mu_D(q_b) - \mu_\infty(q_b)]\ell_p$, rescaled force per monomer $f\ell_p^2$, and rescaled pressure $\propto \rho_b\ell_p$ exerted on the wall. It is evident from Fig. 2a that indeed the effective persistence length $\ell_p(D)$ is the same as that in the bulk (ℓ_p) as long as D exceeds ℓ_p by at least a factor of two. Then a gradual crossover to the relationship $\ell_p(D) \propto \ell_p^2/D$ sets in. The slight scatter of the data from $q_b \approx 0.005$ to 0.02 for strongly confined chains ($D/\ell_p \leq 0.2$) probably indicates problems of efficient sampling in the limit where $\ell_p(D)$ is in the range of several hundred lattice spacings.

Fig. 2b demonstrates that the proper generalization of eqn (14) from flexible to stiff chains is

$$[\mu_D(q_b) - \mu_\infty(q_b)]\ell_p = \text{const}(D/\ell_p)^{-4/3},\ D/\ell_p \gg 1, \tag{22}$$

while for $D/\ell_p < 1$ we find saturation at a constant value (close to unity). Of course, for flexible chains such a regime did not exist (Fig. 1a). Thus using a scaling expression for the free energy per monomer

$$F(q_b, D) = -\frac{1}{N}\ln\frac{Z_N(q_b, D)}{Z_N(q_b, \infty)} = \frac{1}{\ell_p}\tilde{F}(D/\ell_p), \tag{23}$$

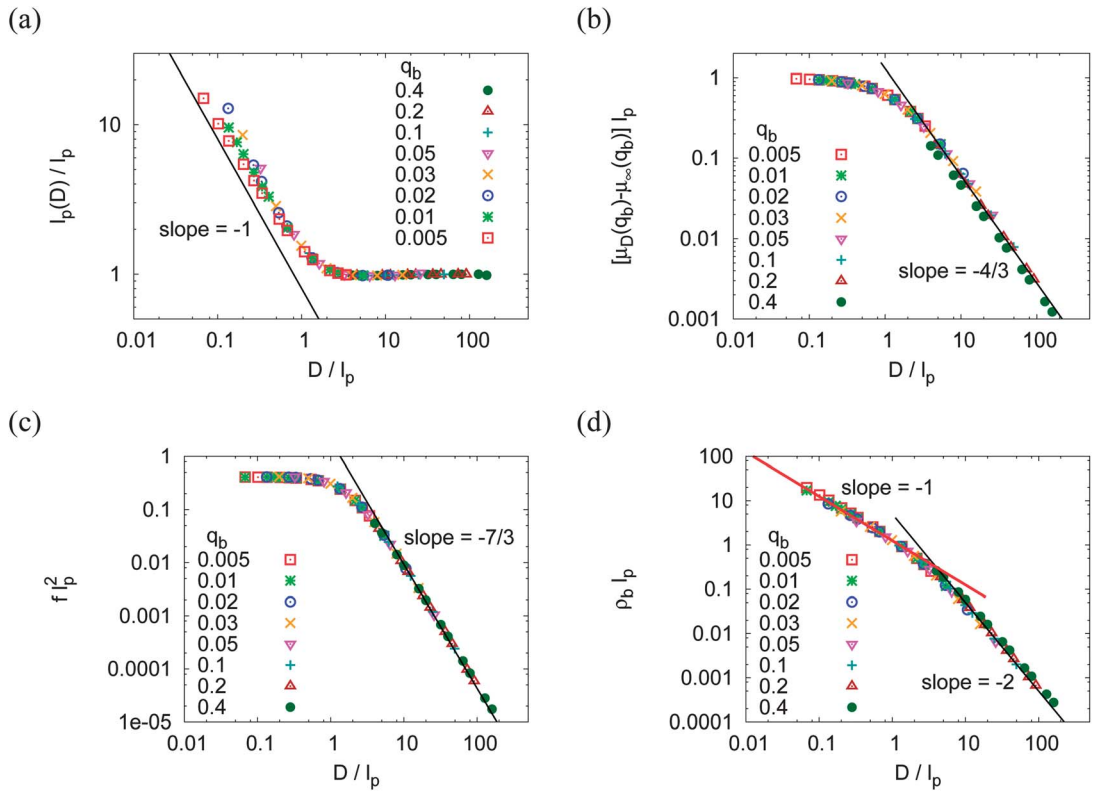

Fig. 2 Log–log plot of the rescaled persistence length $\ell_p(D)/\ell_p$ (a), rescaled fugacity per monomer $[\mu_D(q_b) - \mu_\infty(q_b)]\ell_p$ (b), rescaled force per monomer $f\ell_p^2$ (c), and rescaled monomer density of the wall $\rho_b\ell_p$ (d) *versus* D/ℓ_p. Different choices of q_b are shown in the key of the figures. Straight lines indicate the theoretical exponents. All these data were obtained by extrapolating first data for finite N at fixed q_b and fixed D towards $N \to \infty$ (*cf.* Fig. 3).

which leads to eqn (22), one concludes for the force

$$f = \partial F(q_b,D)/\partial D = \ell_p^{-2}\tilde{F}_f(D/\ell_p), \tilde{F}_f(D/\ell_p \gg 1) \propto (D/\ell_p)^{-7/3}, \quad (24)$$

which is the scaling behavior seen in Fig. 2c. Finally, combining the scaling of the force, eqn (24), with the scaling for the x-component of the end-to-end distance, which we write in generalization of eqn (10) as

$$\langle \Delta x \rangle = N\tilde{X}(D/\ell_p), \quad (25)$$

where $\tilde{X} \approx$ const for $D \ll \ell_p$ and $\tilde{X} \propto (D/\ell_p)^{-1/3}$ for $D \gg \ell_p$. This yields for the pressure (or monomer density on the walls, respectively)

$$\rho_b \propto N(f\ell_p)/\langle \Delta x \rangle = \ell_p^{-1}\tilde{F}_\rho(D/\ell_p) \quad \text{with } \tilde{F}_\rho(D/\ell_p \gg 1) \propto (D/\ell_p)^{-2} \quad (26)$$

This is the behavior seen in Fig. 2d. We remind the reader that this simple scaling behavior applies only in the regime of extremely long chains, so that the regime where D

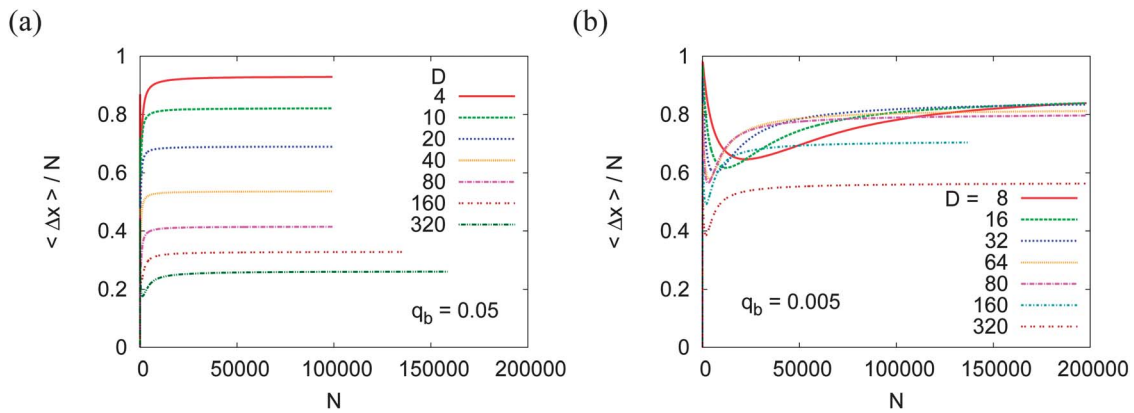

Fig. 3 End-to-end distance per monomer $\langle \Delta x \rangle / N$ in the direction parallel to the confining boundary, plotted *vs.* N for $q_b = 0.05$ (a) and 0.005 (b). Choices of D from $D = 4$ to $D = 320$ are included, as indicated.

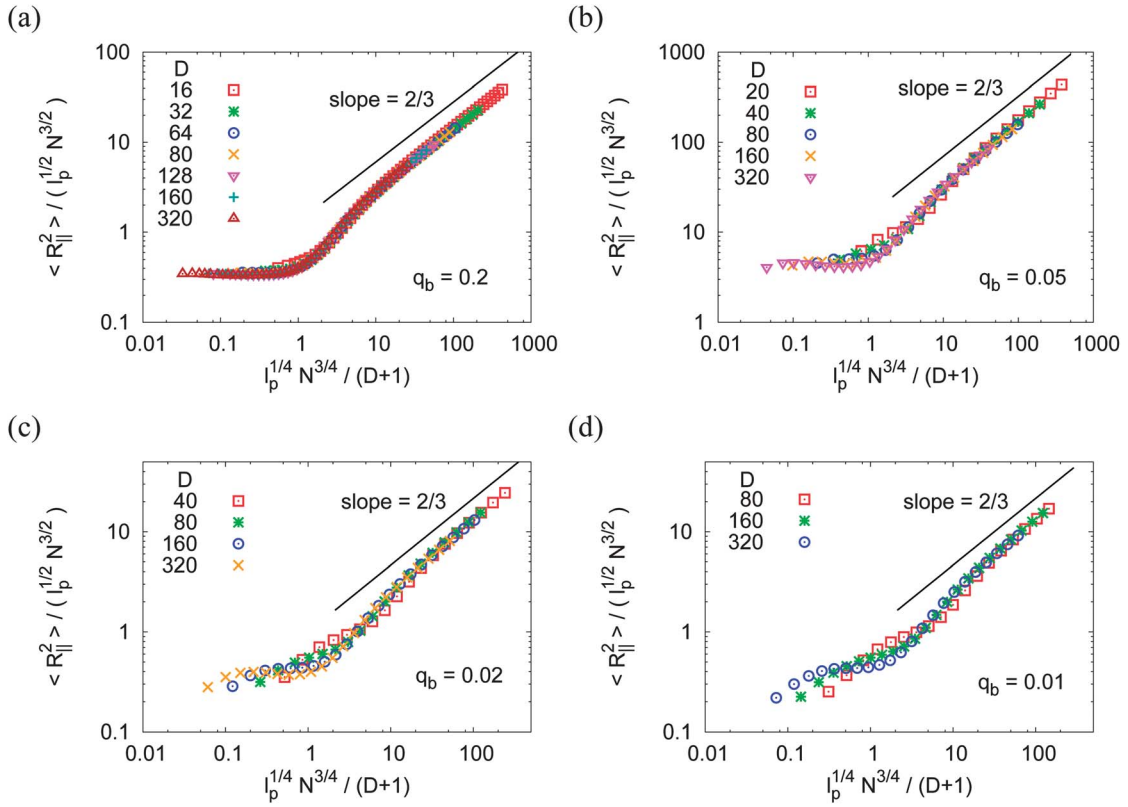

Fig. 4 Log–log plot of $\langle R_{\|}^2\rangle/\ell_p^{1/2}N^{3/2}$ *vs.* $\ell_p^{1/4}N^{3/4}/(D+1)$ for several choices of q_b: 0.2 (a), 0.05 (b), 0.02 (c) and 0.01 (d). Several choices of D are included, as indicated. Straight lines indicate the scaling exponent 2/3 that results with this choice of variables in the blob regime.

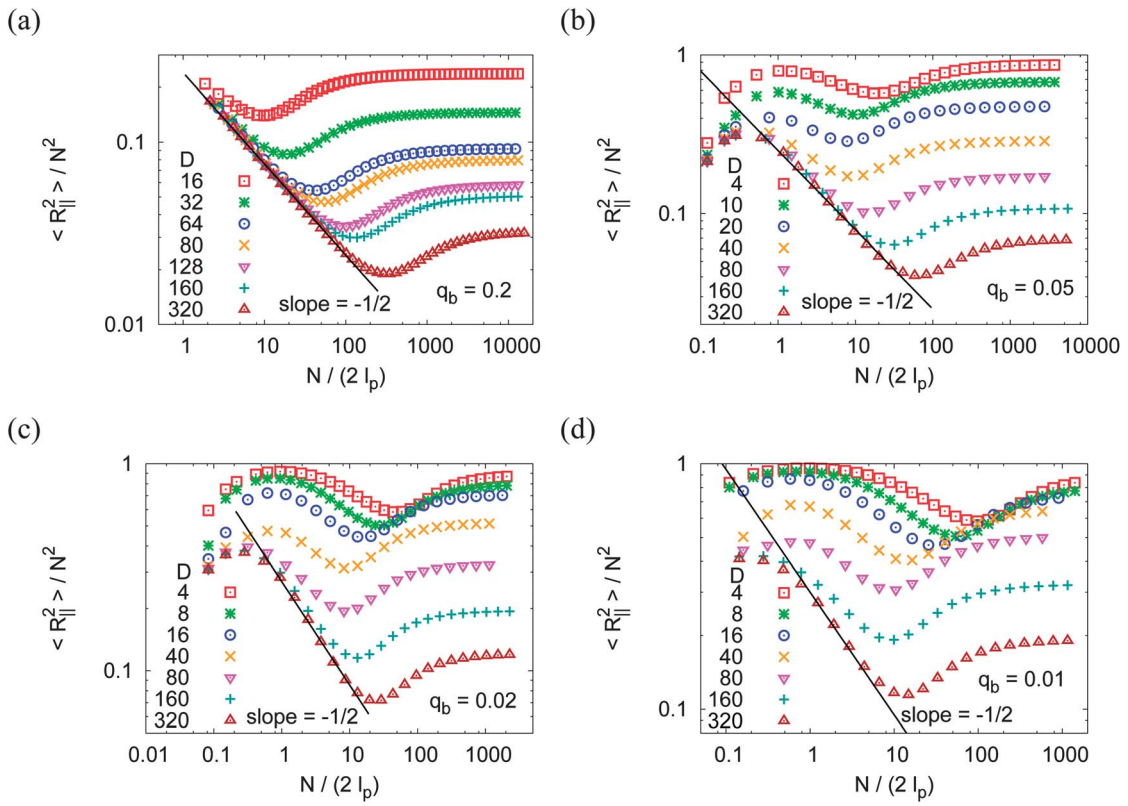

Fig. 5 Log–log plot of $\langle R_{\|}^2\rangle/N^2$ *vs.* $N/(2\ell_p)$ for $q_b = 0.2$ (a), 0.05 (b), 0.02 (c) and 0.01 (d). Many choices of D are included. Straight lines show the relationship $\langle R_{\|}^2\rangle/N^2 \propto N^{-1/2}$, *i.e.* the $d = 2$ SAW behavior $\langle R_{\|}^2\rangle \propto N^{3/2}$.

becomes so large that D is comparable to the extension of a free chain {eqn (9), $\sqrt{\langle R^2\rangle} = \ell_p{}^{1/4}N^{3/4}$} is not yet reached. To avoid any corrections due to such a crossover caused by finite chain length, an extrapolation of suitably normalized data (such as $\langle \Delta x\rangle/N$) towards $N \rightarrow \infty$ has been attempted (Fig. 3). While for not too small q_b (Fig. 3a) the limiting values for $N \rightarrow \infty$ are rather quickly reached, for very small q_b the convergence seems to be problematic for D much smaller than ℓ_p.

3.3 Linear dimensions of confined semi-flexible chains of finite chain length

Being interested also in the crossover from unconfined semi-flexible chains to weakly confined chains for which the blob description, eqn (10), is supposed to hold, we present plots of $\langle R_\parallel{}^2\rangle$ rescaled by the mean square linear dimension of the free semi-flexible chain, $\langle R^2\rangle_0$ {eqn (9)}, as a function of $\sqrt{\langle R^2\rangle_0}/(D+1)$, see Fig. 4. Here, only data for $D \gg \ell_p$ are included, so that the blob-type description should hold. The free chain behavior in this plot shows up as a horizontal plateau for small values of $\sqrt{\langle R^2\rangle_0}/(D+1)$. While for $q_b = 0.2$ this plateau is rather well developed, for smaller q_b deviations from scaling come into play, indicating that strips even wider than $D = 320$ would be needed to reach this regime. The deviation from scaling in the vicinity of $\sqrt{\langle R^2\rangle_0}/(D+1) = 1$ indicates that the crossovers from one regime to the next one are somewhat subtle.

In order to elucidate the various regimes, where $\langle R_\parallel{}^2\rangle \propto N^2$, we plot our data $\langle R_\parallel{}^2\rangle/N^2$ *versus* $N/(2\ell_p)$ for several choices of the stiffness parameter and various strip widths (Fig. 5). One expects that when ℓ_p is large and D is small, one should have a simple rod-behavior $\langle R_\parallel{}^2\rangle = N^2$ for $N/(2\ell_p) < 1$ and this indeed is seen for $q_b = 0.01$ and $D = 4$ or $D = 8$. On the other hand, when $1 < N/(2\ell_p) < 10$ and D is sufficiently large one can see the $d = 2$ SAW behavior, as is obvious from the straight lines in Fig. 5. Then a minimum occurs, and the data rise to another plateau that characterizes the regime where $D < \ell_p$. While the minimum moves monotonously to larger values of $N/(2\ell_p)$ when D increases for small values of ℓ_p (Fig. 5a), the variation of the location of the minimum with D is non-monotonic for large ℓ_p (Fig. 5c and d). It is also interesting to look at the data for $\langle R_\parallel{}^2\rangle/N$ in the case where $D = 40$, and $q_b = 0.01$ (Fig. 5c); the data increase towards a maximum at around $N/(2\ell_p) \approx 0.5$ and then reach a minimum around $(N/2\ell_p) \approx 10$ and then increase towards a plateau, which is only reached for $N/2\ell_p$ of order 1000. Obviously, the interplay of the crossover from rod to SAW (for short enough chains) and the confinement either to a string of blobs or to a somewhat flexible rod (if $D < \ell_p$) is complicated.

A somewhat simpler picture results when we rescale the data with ℓ_p (D) rather than with ℓ_p (Fig. 6). However, this representation also cannot produce perfect data collapse on a master curve either. We also note that in Fig. 5 the ordinate shows only one and half decades, while in Fig. 6 the ordinate shows 5

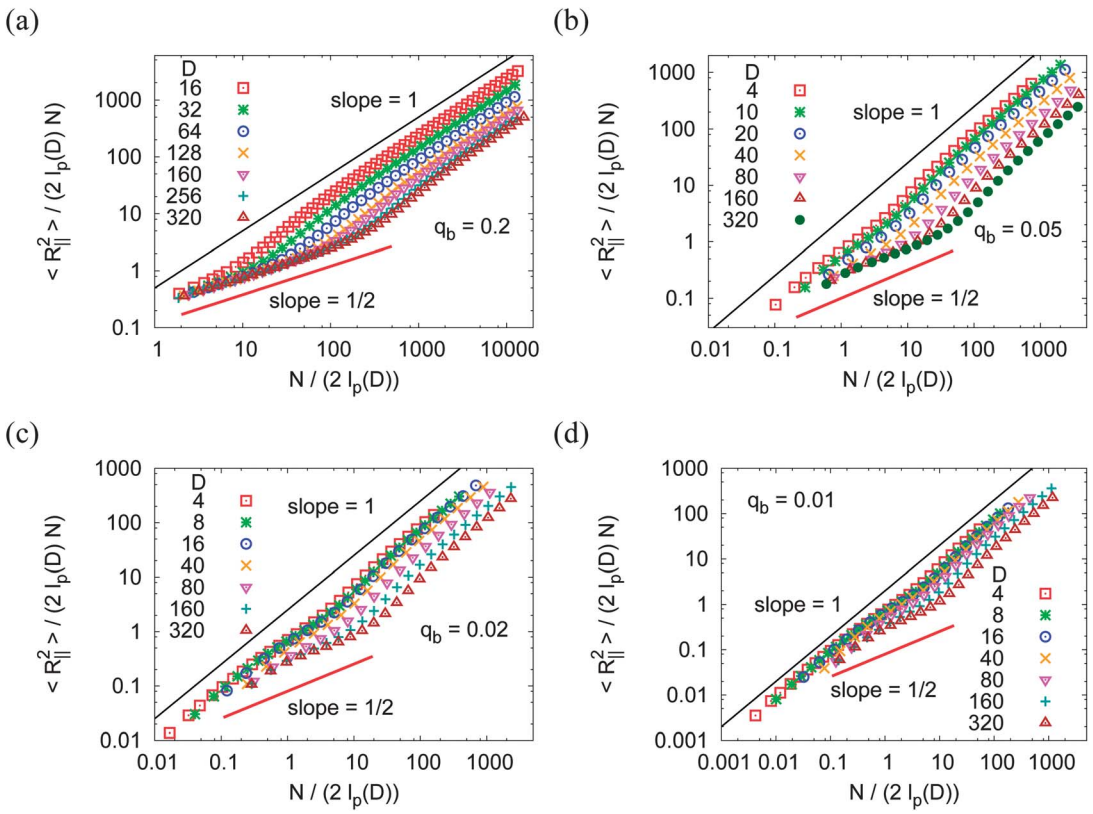

Fig. 6 Log–log plot of $\langle R_\parallel{}^2\rangle/(2\ell_p(D)N)$ *vs.* $N/(2\ell_p(D))$ for $q_b = 0.2$ (a), 0.05 (b), 0.02 (c) and 0.01 (d). Several choices of D are included, as indicated. Straight lines show exponents 1 (for rod-like behavior) and 1/2 (for SAW-like behavior), respectively.

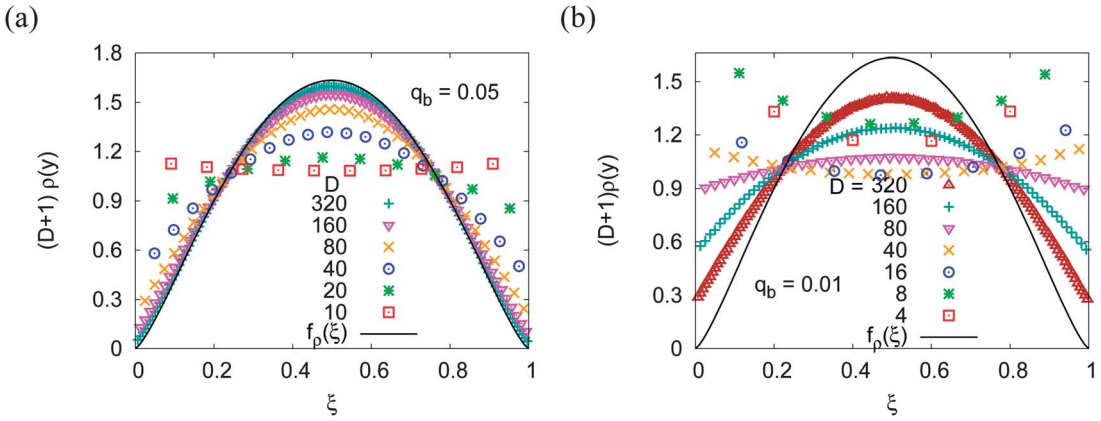

Fig. 7 Rescaled monomer density profile $(D+1)\rho(y)$ *versus* $\xi = y/(D+1)$ for the case $q_b = 0.05$ (a) and $q_b = 0.01$ (b). Several choices of D are included, as indicated. Full curves show eqn (18) with the same amplitude factor as for flexible chains, $A = 10.38$.

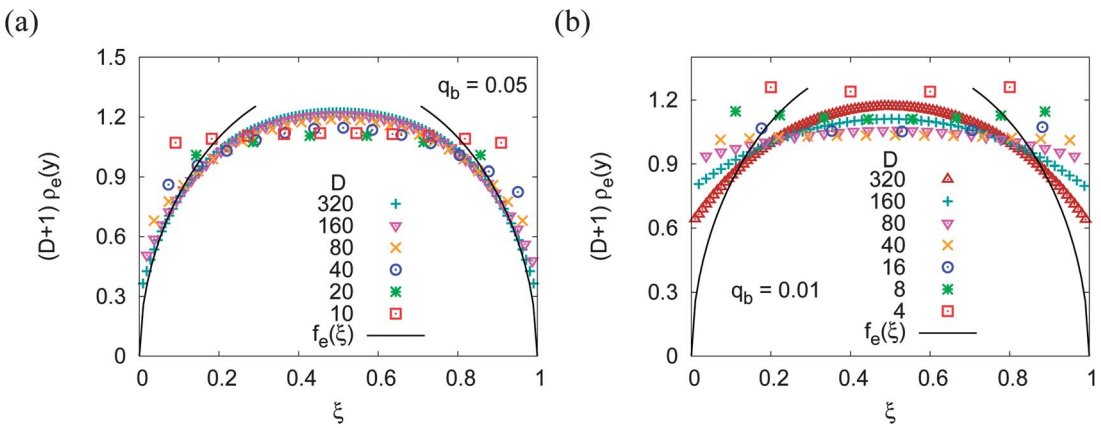

Fig. 8 Rescaled monomer density, $(D+1)\rho_e(y)$ *versus* $\xi = y/(D+1)$, including data for many choices of D, for $q_b = 0.05$ (a) and 0.01 (b). Full curves show eqn (19), with the same amplitude factor A_e as for flexible chains, $A_e = 2.85$.

decades; so differences between the various curves in Fig. 6 are less clearly visible.

3.4 Transverse monomer profiles

In analogy to Fig. 1b, we present scaled monomer profiles across the film in Fig. 7 and in analogy to Fig. 1c, scaled end monomer distributions are given in Fig. 8. Note that here the abscissa variable already is a ratio of lengths, and hence there is no possibility for any rescaling with the persistence length. In fact, for $D \gg \ell_p$, we find that these profiles are quite compatible with the behavior detected for flexible chains. However, when we cross over to the regime $D \leq \ell_p$, the behavior becomes drastically different; both $\rho(y)$ and $\rho_e(y)$ become almost constant, independent of y. In the extreme case, even a slight enhancement of the densities near the walls is seen, in contrast to what one finds for flexible chains. In fact, when a monomer is close to one wall, a relatively long straight piece (almost of length D) running in the y direction perpendicular to the boundaries is possible. Such long straight pieces are preferred if q_b is small. In contrast, for monomers in the center of the strip the longest straight pieces of the chain in the y-direction can only have a length less than $D/2$.

4 Summary and outlook

In this work we have presented a Monte Carlo simulation study of the effects of confinement on the conformation of single semi-flexible chains under good solvent conditions. For simplicity, we consider the two-dimensional case as a first step, since it is already known from studies of the behavior in the bulk that only two types of behavior occur, rod-like behavior for contour lengths of the chain not exceeding its persistence length, and two-dimensional self-avoiding walk behavior ($\langle R^2\rangle_0 \propto N^{3/2}$). Using a simple self-avoiding walk model on the square lattice, where each $\pm 90^\circ$ kink costs an energy ε_b, we can vary the persistence length $\ell_p (\approx 0.61/q_b$ for small $q_b)$ over two orders of magnitude, and chain lengths N up to about $N = 10^5$ are accessible, relying on the PERM algorithm. For this model, the fugacity per monomer μ_∞ (relative to a non-reversal random walk) scales with ℓ_p, *i.e.* $(1-\mu_\infty)\ell_p \approx 1$ for large ℓ_p, and a similar scaling with ℓ_p carries over to describe confinement effects

when the walk is confined in a strip of width D; we find $(\mu_D - \mu_\infty)\ell_p$ to be a function of D/ℓ_p, and the force per monomer f when normalized as $f\ell_p^2$ also is a function of D/ℓ_p, *etc.* (Fig. 2). Particularly interesting is the behavior for $D \leq \ell_p$, when the SAW proceeds mostly in the x-direction so $\sqrt{\langle R_{||}^2\rangle}/N$ stays of order unity (Fig. 5), and one can define an "effective" D-dependent persistence length $\ell_p(D) \propto \ell_p^2/D$, *cf.* Fig. 2a. In our model, no regime occurs where the "deflection length" (eqn (11)) would play any role. For wider strips, $D > \ell_p$, the blob picture (where the chain is a cigar-like string of blobs, $d = 2$ excluded volume statistics applies inside the blob of diameter D) applies, and the scaling behavior is similar to that of flexible chains (compare Fig. 4 to Fig. 1).

We emphasize that our results for $D < \ell_p$ (including also the monomer profiles in Fig. 7 and 8) differ qualitatively from the corresponding predictions based on the Kratky–Porod model, eqn (8). While for $D \gg \ell_p$ the Kratky–Porod description fails due to its neglect of the excluded volume, the question of its validity for $D < \ell_p$ is more subtle; here the excluded volume is not so important, but another crucial difference is that eqn (8) allows for continuous bending, and bond angles can be arbitrarily close to zero, unlike the present lattice model. However, one should not neglect the latter too hastily on the grounds of lattice artefacts. Real polymers such as polyethylene, polystyrene *etc.* have very stiff potentials both for the length ℓ_{cc} of carbon–carbon bonds and the angle θ between them, which can be taken as delta functions at the preferred length $\langle\ell_{cc}\rangle$ and angle $\langle\theta\rangle$, for a very good approximation; the chain flexibility is basically due to the fact that the torsional potential exhibits multiple minima (at $\varphi = 0°, \pm 120°$, for instance). If a piece of an alkane chain exhibits only $\varphi = 0$, it continues essentially straight in the "all *trans*" zig-zag configuration,[36–38] and if only a "*gauche* state" ($\varphi = \pm 120°$) occurs for a bond, the chain proceeds in a different direction. Physically hence ℓ_p corresponds to the typical length of all-*trans* segments, and is controlled by the Boltzmann factor $\exp(-\varepsilon_g/k_BT)$ needed to be used to estimate the density of *gauche* states along the chain. A simple description of this situation is the well known rotational isomeric state (RIS) model,[36–38] of course. The energy parameter ε_g is the analog of our energy parameter ε_b, of course, and while the angles in the RIS model and in alkane chains clearly are not 90°, they are (essentially) discrete, and in this sense our model is more realistic than the Kratky–Porod model allowing for arbitrarily small angles. Of course, there is no direct one-to-one correspondence between our model, where the energy penalty for chain bending is defined in terms of two successive bonds, while in the RIS model the energy penalty refers to the torsional degree of freedom, which can only be defined using three successive bonds. However, there is a qualitative correspondence, *e.g.*, if we would treat an alkane-like chain in the approximation, where interdependence of bond rotational degrees of freedom is neglected, the characteristic ratio could be written as[36] $C_\infty = [(1 + \cos\theta)(1 + \langle\cos\phi\rangle)]/[(1 - \cos\theta)(1 - \langle\cos\phi\rangle)] = 2(1 + \langle\cos\phi\rangle)/(1 - \langle\cos\phi\rangle)$, where we have used that for a tetrahedrally coordinated chain $\cos\theta = 1/3$ (both bond angles θ and bond lengths are taken as rigidly fixed). Using then the standard result for this model[36] $\langle\cos\phi\rangle = (1 - \sigma)/(1 + 2\sigma)$, where $\sigma = \exp(-E_\sigma/k_BT)$ is the Boltzmann factor for the *gauche* states relative to the *trans* state, one finds $C_\infty = 2(2 + \sigma)/(3\sigma) \approx 4/(3\sigma)$ for small σ. Since[36] $\ell_p/\ell = (C_\infty + 1)/2$ one finds that for small σ (necessary to have stiff chains) $\ell_p/\ell \approx (2/3)\sigma^{-1} = (2/3)\exp(E_\sigma/k_BT)$, which is the analog of our result $\ell_p/\ell \approx 0.61\exp(\varepsilon_b/k_BT)$ quoted at the end of Section 2. Of course, one should be aware that in real alkane chains successive torsional angles are not independent of each other, so a really quantitative application of our model to real polymers would be premature. For systems such as microtubuli where ℓ_p is in the range of μm, on the other hand, it is obvious that such atomistic effects do not play any role, and then eqn (8) presumably is a reasonable description. In our view, it matters whether or not the persistence length is orders of magnitude larger than this atomistic length of chemical bonds along the chain. Thus eqn (8) clearly is unsuitable to describe confinement effects on single-stranded DNA, for confined double-stranded DNA eqn (8) would work if all hydrogen bonds remain intact.

Of course, for a direct application of our simulations to a real system one would have to consider a strongly adsorbed polymer on a surface of finite extent in one direction (*e.g.* a terrace of width D on a stepped surface, under conditions where it is too energetically unfavorable for the polymer to cross a terrace boundary.) Clearly, there is a lot of interest in polymers confined in cylindrical tubes or in slits bound by planar walls; we hope to report on an extension of the present work to $d = 3$ dimensions in the future.

Acknowledgements

We are grateful to the Deutsche Forschungsgemeinschaft (DFG) for support under Grant no. SFB 625/A3, and to the John von Neumann Institute for Computing (NIC Jülich) for a generous grant of computer time.

References

1 J. O. Tegenfeldt, C. Prinz, H. Cao, S. Chou, W. W. Reisner, R. Riehn, Y. M. Wang, E. C. Cox, J. C. Sturm, P. Silberzan and R. H. Austin, *Proc. Natl. Acad. Sci. U. S. A.*, 2004, **101**, 10979–10983.
2 W. Reisner, K. J. Morton, R. Riehn, Y. M. Wang, Z. Yu, M. Rosen, J. C. Sturm, S. Y. Chou, E. Frey and R. H. Austin, *Phys. Rev. Lett.*, 2005, **94**, 196101.
3 K. Jo, D. M. Dhingra, T. Odijk, J. J. de Pablo, M. D. Graham, R. Runnheim, D. Forrest and D. C. Schwartz, *Proc. Natl. Acad. Sci. U. S. A.*, 2007, **104**, 2673–2578.
4 K. Shin, S. Obukhov, J.-T. Chen, J. Huh, Y. Hwang, S. Mok, P. Dobriyal, P. Thiyagarajan and T. P. Russell, *Nat. Mater.*, 2007, **6**, 961–965.
5 D. J. Bonthuis, C. Meyer, D. Stein and C. Dekker, *Phys. Rev. Lett.*, 2008, **101**, 108303.
6 P.-K. Lin, K.-H. Lin, C.-C. Fu, K.-C. Lee, P.-K. Wei, W.-W. Pai, P.-H. Tsao, Y.-L. Chen and W. S. Fann, *Macromolecules*, 2009, **42**, 1770–1774.
7 J. Tang, S. L. Levy, D. W. Trahan, J. J. Jones, H. G. Craighead and P. S. Doyle, *Macromolecules*, 2010, **43**, 7368–7377.

8 H. Uemura, M. Ichikawa and Y. Kimura, *Phys. Rev. E: Stat., Nonlinear, Soft Matter Phys.*, 2010, **81**, 051801.
9 W. Helfrich, *Z. Naturforsch., A: Phys., Phys. Chem., Kosmophys.*, 1978, **33**, 305–315.
10 A. R. Khokhlov and A. N. Semenov, *Phys. A*, 1981, **108**, 546–556.
11 A. R. Khokhlov and A. N. Semenov, *Phys. A*, 1982, **112**, 605–614.
12 T. Odijk, *Macromolecules*, 1983, **16**, 1340–1343.
13 W. Helfrich and R. M. Servuss, *Nuovo Cimento Soc. Ital. Fis., D*, 1984, **3**, 137–151.
14 W. Helfrich and W. Harbich, *Chem. Scr.*, 1985, **25**, 32.
15 T. Odijk, *Macromolecules*, 1986, **19**, 2313–2329.
16 M. Dijkstra, D. Frenkel and H. N. W. Lekkerkerker, *Phys. A*, 1993, **193**, 374–393.
17 T. W. Burkhardt, *J. Phys. A*, 1997, **30**, L167–L172.
18 R. Granek, *J. Phys. II*, 1997, **7**, 1761–1788.
19 L. Harnau and P. Reineker, *Phys. Rev. E: Stat. Phys., Plasmas, Fluids, Relat. Interdiscip. Top.*, 1999, **60**, 4671.
20 D. J. Bicout and T. W. Burkhardt, *J. Phys. A*, 2001, **34**, 5745–5750.
21 J. Z. Y. Chen and D. E. Sullivan, *Macromolecules*, 2006, **39**, 7769–7773.
22 Y. Yang, T. W. Burkhardt and G. Gompper, *Phys. Rev. E: Stat., Nonlinear, Soft Matter Phys.*, 2007, **76**, 011804.
23 P. Levi and K. Mecke, *Europhys. Lett.*, 2007, **78**, 38001.
24 F. Wagner, G. Lattanzi and E. Frey, *Phys. Rev. E: Stat., Nonlinear, Soft Matter Phys.*, 2007, **75**, 050902.
25 T. Odijk, *Phys. Rev. E: Stat., Nonlinear, Soft Matter Phys.*, 2008, **77**, 060901(R).
26 T. W. Burkhardt, Y. Yang and G. Gompper, *Phys. Rev. E: Stat., Nonlinear, Soft Matter Phys.*, 2010, **82**, 041801.
27 T. Thüroff, P. Wagner and E. Frey, *Europhys. Lett.*, 2010, **91**, 38004.
28 F. Thüroff, B. Obermayer and E. Frey, *Phys. Rev. E: Stat., Nonlinear, Soft Matter Phys.*, 2011, **83**, 021802.
29 Y.-L. Chen, M. D. Graham, J. J. de Pablo, G. C. Randall, M. Gupta and P. S. Doyle, *Phys. Rev. E: Stat., Nonlinear, Soft Matter Phys.*, 2004, **70**, 060901(R).
30 P. Cifra, *J. Chem. Phys.*, 2009, **131**, 224903.
31 P. Cifra, Z. Benkova and T. Bleha, *J. Phys. Chem. B*, 2009, **113**, 1843–1851.
32 P. Cifra, *J. Chem. Phys.*, 2012, **136**, 024902.
33 P. G. de Gennes, *Scaling Concepts in Polymer Physics*, Cornell Univ. Press, Ithaca, 1979.
34 J. C. Le Guillou and J. Zinn-Justin, *Phys. Rev. B: Condens. Matter Mater. Phys.*, 1980, **21**, 3976–3998.
35 M. Daoud and P. G. de Gennes, *J. Phys.*, 1977, **38**, 85–93.
36 P. J. Flory, *Statistical Mechanics of Chain Molecules*, Interscience, New York, 1969.
37 H. Yamakawa, *Modern Theory of Polymer Solutions*, Harper and Row, London, 1971.
38 A. Yu. Grosberg and A. R. Khokhlov, *Statistical Mechanics of Macromolecules*, AIP Press, New York, 1994.
39 H.-P. Hsu, W. Paul and K. Binder, *Macromolecules*, 2010, **43**, 3094–3102.
40 L. Schäfer, A. Ostendorf and J. Hager, *J. Phys. A: Math. Gen.*, 1999, **32**, 7875–7899.
41 H.-P. Hsu, W. Paul and K. Binder, *EPL*, 2011, **95**, 68004.
42 O. Kratky and G. Porod, *J. Colloid Sci.*, 1949, **4**, 35–70.
43 T. R. Strick, M.-N. Dessinges, G. Charvin, N. H. Dekker, J.-F. Allemand, D. Bensimon and V. Croquette, *Rep. Prog. Phys.*, 2003, **66**, 1–45.
44 P. Grassberger, *Phys. Rev. E: Stat. Phys., Plasmas, Fluids, Relat. Interdiscip. Top.*, 1997, **56**, 3682–3693.
45 H.-P. Hsu and P. Grassberger, *J. Stat. Phys.*, 2011, **144**, 597–637.
46 H.-P. Hsu and K. Binder, *J. Chem. Phys.*, 2012, **136**, 024901.
47 H.-P. Hsu and P. Grassberger, *Eur. Phys. J. B*, 2003, **36**, 209–214.
48 J. L. Cardy and S. Redner, *J. Phys. A: Math. Gen.*, 1984, **17**, L933–L938.

